Evaluating the influence of mechanical stress on anticancer treatments through a multiphase porous media model

Evaluating the influence of mechanical stress on anticancer treatments through a multiphase porous media model

Pietro Mascheroni[a], Daniela Boso[a], Luigi Preziosi[b], Bernhard A. Schrefler[c,#]

a Dipartimento di Ingegneria Civile, Edile ed Ambientale, Università di Padova, Via Marzolo 9, 35131 Padova, Italy

b Dipartimento di Matematica, Politecnico di Torino, Corso Duca degli Abruzzi 24, 10124 Torino, Italy

c Da compilare

corresponding author

Highlights

- Low-proliferating cell populations contribute to drug resistance
- Compressive stresses act on tumors by inhibiting cell proliferation
- We analyze the combined effects of drug action and mechanical compression
- Mechanical compression of tumors may compromise drug efficacy

Abstract

Drug resistance is one of the leading causes of poor therapy outcomes in cancer. As several chemotherapeutics are designed to target rapidly dividing cells, the presence of a low-proliferating cell population contributes significantly to treatment resistance. Interestingly, recent studies have shown that compressive stresses acting on tumor spheroids are able to hinder cell proliferation, through a mechanism of growth inhibition. However, studies analyzing the influence of mechanical compression on therapeutic treatment efficacy have still to be performed. In this work, we start from an existing mathematical model for avascular tumors, including the description of mechanical compression. We introduce governing equations for transport and uptake of a chemotherapeutic agent, designed to target cell proliferation. Then, model equations are adapted for tumor spheroids and the combined effect of compressive stresses and drug action is investigated. Interestingly, we find that the variation in tumor spheroid volume, due to the presence of a drug targeting cell proliferation, considerably depends on the compressive stress level of the cell aggregate. Our results suggest that mechanical compression of tumors may compromise the efficacy of chemotherapeutic agents. In particular, a drug dose that is effective in reducing tumor volume for stress-free conditions may not perform equally well in a mechanically compressed environment.

Keywords

Cancer; Chemotherapy; Tumor Spheroids; Mathematical Model; Mechanical Compression

1. Introduction

A major hurdle to chemotherapy success is resistance of tumor cells to therapeutic agents. In general, resistance may arise as an intrinsic cellular response or as a result of drug treatment (Zahreddine and Borden, 2013). It is known that the presence of a low-proliferating cell population is one of the leading factors contributing to drug resistance in solid tumors (Mueller-Klieser, 2000; Trédan et al., 2007). In fact, several chemotherapeutic agents are effective against rapidly dividing cells. Moreover, as certain normal tissues display high rates of cellular divisions (such as the gut mucosal and bone marrow cells), there exists a toxicity limit determining the maximum administrable drug dose (Dawidczyk et al., 2014).

Such resistance mechanisms, dependent on the proliferative activity of tumor cells, are generally investigated *in vitro* through the use of three-dimensional cell aggregates, known as tumor spheroids (Vinci et al., 2012). Contrary to conventional monolayer cultures, tumor spheroids display heterogeneous cell populations, including quiescent and necrotic cells, together with resistant phenomena to different chemotherapeutic drugs (Mikhail et al., 2013). Cell quiescence results both from the lack of nutrients and growth factors within the tumor, and from adhesion interactions between cells of the same type. Indeed, cells from healthy tissues display a mechanism of “contact inhibition” that regulates proliferation in a crowded environment (Abercrombie and Ambrose, 1962). This mechanism allows the cells to stop proliferation as soon as certain cell densities are reached at a given site. Tumor cells exhibit an analogous behavior, even though to a significant lesser extent than their healthy counterpart, and with more relevance in three-dimensional cultures than in monolayers (St Croix et al., 1998).

The biochemical pathways underlying contact inhibition are still an active area of research. They are linked to adhesive interactions between neighboring cells, mediated by adhesion proteins such as cadherins. Moreover, these mechanisms include a series of proteins involved in cell cycle regulation. To this regard, the G1 checkpoint, also known as the restriction point (R), represents a fundamental step in the cell cycle, controlling cell commitment to mitosis (Planas-Silva and Weinberg, 1997). Regulation of this cell checkpoint depends on the retinoblastoma protein (pRb). In particular, the

hypo-phosphorylated form of pRb prevents progression from the G1 to the S phase of the cell cycle, inhibiting cell duplication. On the other hand, phosphorylation of pRb leads to its inactivation allowing the cell to undergo mitosis. Phosphorylation of pRb depends on cyclin-dependent kinases (cdks), which in turn are subject to the action of cyclins (Dietrich et al., 1997). Finally, the activity of the whole complex is further regulated by several inhibitor proteins, in particular the cyclin-dependent kinase inhibitor p27 (Hengst et al., 1994; Polyak et al., 1994). Interestingly, an over-expression of this protein has been observed following cell-cell contact in three-dimensional cultures, as compared to monolayers (St Croix et al., 1998, 1996; Xing et al., 2005). The adhesive interaction between cells inside tumor spheroids leads to upregulation of p27, which results in cell arrest in a quiescent phase of the cycle. Recently, the expression of p27 has been investigated through a series of experiments involving mechanical compression of three-dimensional cell aggregates (Delarue et al., 2014). Results show that a controlled compressive stress on tumor spheroids inhibits cell proliferation by an over-expression of p27, blocking the cancerous cells at the restriction point of the cell cycle.

At the beginning of this introduction, we have observed that the presence of a non-proliferating cellular fraction has important consequences on the therapeutic efficacy of different chemotherapeutic agents. Notably, previous works have shown that a reduction in p27 expression in tumor spheroids could lead to better outcomes in terms of drug performance (St Croix et al., 1998, 1996; Xing et al., 2005). However, experiments quantifying the influence of mechanical stress on drug efficacy have still to be performed. Note that, interestingly, the compressive stresses that can be induced in tumor spheroids are of the same order of magnitude of those measured *in vivo* (Butcher et al., 2009; Fernández-Sánchez et al., 2015; Stylianopoulos et al., 2012), in the range of a few kPa.

Phenomena concerning the mechanisms of drug action, as well as the mechanical characterization of the state of a tissue, are difficult to investigate from a pure biological and biochemical framework. To this end, mathematical models provide a valuable tool for establishing which of the biophysical features of the tumor and the stroma are responsible for the observed behaviors. In the last years, several review papers discussing different approaches to cancer modeling have been published (Altrock et al., 2015; Byrne, 2010; Preziosi and Tosin, 2009; Sciumè et al., 2013). Some models describe the action of a therapeutic agent on tumor spheroids (see for example (Frieboes et al., 2009; Goodman et al., 2008; Ward and King, 2003)), whereas others take into account *in vivo*

settings, as in (Hossain et al., 2012; Kim et al., 2013; Mpekris et al., 2015). There are also models addressing the effects of mechanical stress on tumor development, such as those in (Kim et al., 2011; Loessner et al., 2013; Stylianopoulos et al., 2012). However, to the authors' knowledge, there is a lack of mathematical models focusing on the interactions between anticancer agents and the mechanical environment surrounding the tumor.

The aim of this work is to develop a theoretical framework that is able to take into account these interactions, providing new insights into mechanics-mediated drug resistance. In the following, we specialize our study to tumor spheroids. We address the effects of a chemotherapeutic agent, supposed to target cell proliferation, on these cell aggregates. Then, we evaluate the influence of mechanical compression on treatment efficacy.

The remainder of this work is organized as follows. Section 2 describes the mathematical model; the governing equations are presented, together with the assumed constitutive relations and parameter values. In Section 3 we report the results of the model. We start from the effects of different drug concentrations on the spheroid growth curve. Then, we consider a range of mechanical pressures acting on the spheroid surface and investigate their interactions with the treatment. Finally, we test different mathematical expressions for the drug-induced cell death term. Section 4, at the end, presents some concluding remarks.

2. Mathematical model

2.1 Governing equations

We build upon the mathematical model in (Mascheroni et al., 2016) to describe the transport of chemotherapeutic agents within an avascular tumor. The tumor is modeled as a biphasic porous material, and the governing equations are derived from porous media theory. We denote by t the solid phase of the porous medium, constituted by tumor cells (TCs) and ECM. The interstitial fluid (IF) constitutes the fluid phase (ℓ), which permeates the pores of the cellular scaffold. In our description, TCs are divided into living (Lt) and necrotic (Nt) fractions. In addition, we assume that the IF carries a nutrient, namely oxygen (ox), and a drug (ch). We consider a saturated material, where the IF fills all the voids of the porous medium. This results in the saturation constraint:

$$\varepsilon^t + \varepsilon^\ell = 1 \tag{1}$$

where ε^{α} denotes the volume fraction of phase α ($\alpha = t, \ell$). The mass balance equations for the phases in the biphasic system are given by:

$$\frac{\partial\left(\varepsilon^{t}\rho^{t}\right)}{\partial t} + \operatorname{div}\left(\varepsilon^{t}\rho^{t}\mathbf{v}^{t}\right) = \underset{g}{M}^{\ell\to t} - \underset{d}{M}^{t\to\ell} \tag{2}$$

$$\frac{\partial\left(\varepsilon^{\ell}\rho^{\ell}\right)}{\partial t} + \operatorname{div}\left(\varepsilon^{\ell}\rho^{\ell}\mathbf{v}^{\ell}\right) = -\underset{g}{M}^{\ell\to t} + \underset{d}{M}^{t\to\ell} \tag{3}$$

where ρ^{α} is the true mass density and $\mathbf{v}^{\alpha}$ the velocity of the α phase ($\alpha = t, \ell$). Here $\underset{g}{M}^{\ell\to t}$ is the term responsible for mass exchange between IF and TCs, dependent on cell proliferation; $\underset{d}{M}^{t\to\ell}$ represents instead mass exchange between TCs and IF resulting from cell death and their following degradation. Oxygen and drug are described as species dissolved into the IF, and their mass balance reads:

$$\frac{\partial\left(\varepsilon^{\ell}\rho^{\ell}\omega^{ox}\right)}{\partial t} + \operatorname{div}\left(\varepsilon^{\ell}\rho^{\ell}\omega^{ox}\mathbf{v}^{\ell}\right) - \operatorname{div}\left[\varepsilon^{\ell}\rho^{\ell}D^{ox}\operatorname{grad}\left(\omega^{ox}\right)\right] = -\underset{ox}{M}^{ox\to t} \tag{4}$$

$$\frac{\partial\left(\varepsilon^{\ell}\rho^{\ell}\omega^{ch}\right)}{\partial t} + \operatorname{div}\left(\varepsilon^{\ell}\rho^{\ell}\omega^{ch}\mathbf{v}^{\ell}\right) - \operatorname{div}\left[\varepsilon^{\ell}\rho^{\ell}D^{ch}\operatorname{grad}\left(\omega^{ch}\right)\right] = -\underset{ch}{M}^{ch\to t} \tag{5}$$

where ω^{β} denotes the mass fraction of species β and D^{β} is its diffusion coefficient ($\beta = ox, ch$). The terms $\underset{ox}{M}^{ox\to t}$ and $\underset{ch}{M}^{ch\to t}$ represent oxygen and drug uptake by TCs, respectively. We describe the evolution for living and necrotic TCs through the system:

$$\frac{\partial\left(\varepsilon^{t}\rho^{t}\omega^{Lt}\right)}{\partial t} + \operatorname{div}\left(\varepsilon^{t}\rho^{t}\omega^{Lt}\mathbf{v}^{t}\right) = -\varepsilon^{t}r^{Nt} + \underset{g}{M}^{\ell\to t} \tag{6}$$

$$\frac{\partial\left(\varepsilon^{t}\rho^{t}\omega^{Nt}\right)}{\partial t} + \operatorname{div}\left(\varepsilon^{t}\rho^{t}\omega^{Nt}\mathbf{v}^{t}\right) = \varepsilon^{t}r^{Nt} - \underset{d}{M}^{t\to\ell} \tag{7}$$

where we have denoted by ω^{Lt} and ω^{Nt} the mass fractions of living and necrotic cells, respectively. Here $\varepsilon^{t}r^{Nt}$ is an intra-phase mass exchange term, commonly denoted as reaction term, accounting for the transfer of TCs from living to necrotic. Note that, by summing (6) and (7) we obtain (2) assuming that:

$$\omega^{Lt} = 1 - \omega^{Nt} \tag{8}$$

Following porous media theory (Lewis and Schrefler, 1998; Pinder and Gray, 2008), the mechanical stress exerted on the solid phase is described through the effective stress tensor $\mathrm{t}^{t}_{\mathrm{eff}}$ given by:

$$\mathrm{t}^{t}_{\mathrm{eff}} = \mathrm{t}^{t} + \alpha_B p^{\ell} \mathrm{I} \tag{9}$$

where I is the unit tensor, t^{t} the total stress tensor, p^{ℓ} is the fluid pressure in the interstitial fluid and α_B is Biot's coefficient defined by:

$$\alpha_B = 1 - \frac{K}{K_T}, \tag{10}$$

with K bulk modulus of the unsaturated skeleton and K_T bulk modulus of the solid phase. Then, we can state the linear momentum balance law for the tissue as (Lewis and Schrefler, 1998):

$$\mathrm{div}\mathrm{t}^{t} = \mathrm{div}\left(\mathrm{t}^{t}_{\mathrm{eff}} - \alpha_B p^{\ell} \mathrm{I}\right) = 0 \tag{11}$$

Note that in (9) the tensile components of the stress tensors t^{t} and $\mathrm{t}^{t}_{\mathrm{eff}}$ are assumed positive.

2.2 Constitutive relations

In (Mascheroni et al., 2016), constitutive relationships for the effective stress and the mass transfer terms have been formulated. In particular, we have assumed the following form for the effective stress:

$$\mathrm{t}^{t}_{\mathrm{eff}} = -\Sigma\left(\varepsilon^{t}\right)\mathrm{I} \tag{12}$$

with $\Sigma\left(\varepsilon^{t}\right)$ given by:

$$\Sigma\left(\varepsilon^{t}\right) = \begin{cases} \alpha\left(\varepsilon^{t} - \varepsilon_0^{t}\right)^2 \left[\dfrac{1-\varepsilon_n^{t}}{\left(1-\varepsilon^{t}\right)^{\beta}} - \dfrac{1}{\left(1-\varepsilon^{t}\right)^{\beta-1}}\right], & \text{if } \varepsilon^{t} > \varepsilon_0^{t} \\ 0, \quad \text{otherwise} \end{cases} \tag{13}$$

This pseudo-potential law describes cells that do not interact if their volume fraction is below a given threshold (ε_0^t). Otherwise, they start to interact and develop attraction forces as long as their volume fraction is below a control value (ε_n^t). Finally, if TCs become too densely packed exhibiting a high volume fraction, they start to repel each other. This behavior is schematized in Figure 1. In the following we will denote by $\Sigma'(\varepsilon^t)$ the derivative of $\Sigma(\varepsilon^t)$ with respect to ε^t.

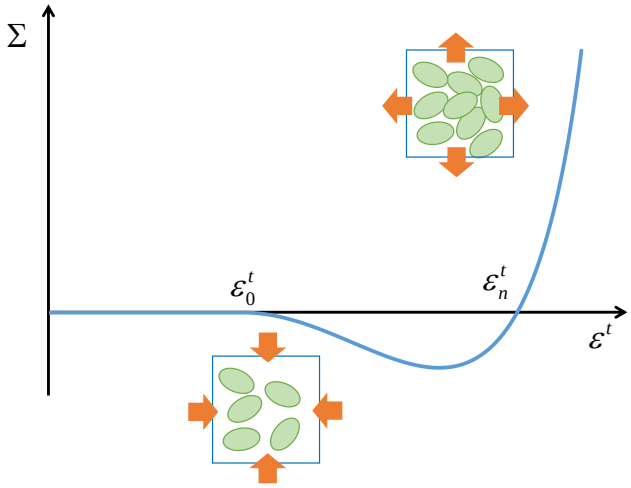

Figure 1 Schematic for the stress function $\Sigma\left(\varepsilon^t\right)$, depicting the behavior of cells at different volume fractions.

The mass exchange terms in equation (2) represent TC growth and death, respectively. The first term describes cell proliferation and depends on the transfer of mass between the IF and the living fraction of the tumor. It takes the form:

$$\underset{g}{\overset{\ell\to t}{M}} = \gamma_g^t \left\langle \frac{\omega^{ox} - \omega_{crit}^{ox}}{\omega_{env}^{ox} - \omega_{crit}^{ox}} \right\rangle_+ \left(1 - \delta_1 \frac{\langle \Sigma \rangle_+}{\langle \Sigma \rangle_+ + \delta_2} \right) \omega^{Lt} \varepsilon^t \tag{14}$$

here the coefficient γ_g^t accounts for oxygen uptake and for mass of IF that becomes tumor due to cell growth; ω_{crit}^{ox} is the critical mass fraction of oxygen, below which growth is inhibited, and ω_{env}^{ox} is the reference mass fraction of oxygen in the environment. The Macaulay brackets $\langle\cdot\rangle_+$ indicate the positive value of their argument: since the oxygen mass fraction ω^{ox} within the tumor can only be

equal to or smaller than ω_{env}^{ox}, the brackets will return a number between one ($\omega^{ox} = \omega_{env}^{ox}$) and zero ($\omega^{ox} < \omega_{env}^{ox}$). The term in round squares describes growth inhibition by mechanical stress. The constants δ_1 and δ_2 (with $\delta_1 < 1$) regulate the action of mechanical stress on cell proliferation and, together with the term $\langle \Sigma \rangle_+$, model the inhibitory effect of compression on tumor cells proliferation (Cheng et al., 2009; Helmlinger et al., 1997; Montel et al., 2012).

The rate of TC death in equation (2) is given by:

$$\underset{d}{M}^{t\to\ell} = \underset{d,ly}{M}^{t\to\ell} + \underset{d,ch}{M}^{t\to\ell} \tag{15}$$

where the two contributions are related to cell lysis and drug action. In particular, the first term is given by:

$$\underset{d,ly}{M}^{t\to\ell} = \lambda_\ell^t \omega^{Nt} \varepsilon^t \tag{16}$$

where the coefficient λ_ℓ^t takes into account cellular degradation and mass conversion of necrotic cells into IF. The second term takes the form:

$$\underset{d,ch}{M}^{t\to\ell} = f_{ch} \lambda_{ch}^t \omega^{ch} \omega^{Lt} \varepsilon^t \tag{17}$$

Here λ_{ch}^t accounts for the rate of drug-induced cell death. The function f_{ch} is related to the mechanism of action of the drug that is considered. Since we are interested in drugs that target TC proliferation, we assume f_{ch} to depend on the growth term in (14):

$$f_{ch}\left(\omega^{ox}, \Sigma\right) = \frac{M_g^{\ell\to t}}{\max\left(M_g^{\ell\to t}\right)} = \left\langle \frac{\omega^{ox} - \omega_{crit}^{ox}}{\omega_{env}^{ox} - \omega_{crit}^{ox}} \right\rangle_+ \left(1 - \delta_1 \frac{\langle \Sigma \rangle_+}{\langle \Sigma \rangle_+ + \delta_2}\right) \tag{18}$$

where we highlight the dependence of f_{ch} on both the nutrient mass fraction ω^{ox} and the mechanical stress Σ. In this way, the drug is most effective on the TCs that are well nourished and not compressed. Note that, depending on the particular drug that is considered, different choices for f_{ch} are possible (for example, in this framework it is possible to simulate drugs targeting hypoxia or specific cellular species in the tumor).

The rate of necrosis of living tumor cells in equation (6) is described by:

202 $$\varepsilon^t r^{Nt} = \gamma_n^t \left\langle \frac{\omega_{crit}^{ox} - \omega^{ox}}{\omega_{env}^{ox} - \omega_{crit}^{ox}} \right\rangle_+ \omega^{Lt} \varepsilon^t \tag{19}$$

203 where the parameter γ_n^t regulates the rate of cell necrosis. The terms in the Macaulay brackets
204 represent cell death by lack of nutrients.

205 During growth, TCs consume nutrients from the IF, a process that is described by the mass exchange
206 term in equation (4):

207 $$\underset{ox}{\overset{ox\to t}{M}} = \gamma_0^t \frac{\omega^{ox}}{\omega^{ox} + c^{ox}} \omega^{Lt} \varepsilon^t \tag{20}$$

208 This expression accounts for the dependence of oxygen consumption on its local level in the tumor.
209 The coefficients γ_0^t and c^{ox} represent the order of magnitude of oxygen uptake and the oxygen
210 mass fraction at which consumption is reduced by half, respectively.

211 Finally, the mass transfer term related to drug uptake in equation (5) takes the form:

212 $$\underset{ch}{\overset{ch\to t}{M}} = \gamma_{ch}^t \omega^{ch} \omega^{Lt} \varepsilon^t \tag{21}$$

213 where we assumed the simplest kinetics for drug uptake (i.e. linear), with γ_{ch}^t accounting for the
214 drug uptake rate by living TCs (Frieboes et al., 2009; Weinberg et al., 2007).

215

216 *2.3 Model specialization to tumor spheroids*

217 The equations of the model can be specialized to the case of tumor spheroids, following a similar
218 procedure to that in (Mascheroni et al., 2016). The resulting system for the TC volume fraction,
219 necrotic mass fraction, and oxygen and drug mass fractions can be summarized as:

220 $$\frac{\partial \varepsilon^t}{\partial t} - \frac{1}{r^2}\frac{\partial}{\partial r}\left(r^2 \varepsilon^t \frac{k}{\mu^\ell} \Sigma' \frac{\partial \varepsilon^t}{\partial r} \right) - \frac{1}{\rho}\left(\underset{g}{\overset{\ell\to t}{M}} - \underset{d}{\overset{t\to \ell}{M}} \right) = 0 \tag{22}$$

221 $$\frac{\partial \left(\omega^{Nt} \varepsilon^t \right)}{\partial t} - \frac{1}{r^2}\frac{\partial}{\partial r}\left(r^2 \varepsilon^t \omega^{Nt} \frac{k}{\mu^\ell} \Sigma' \frac{\partial \varepsilon^t}{\partial r} \right) - \frac{1}{\rho}\left(\varepsilon^t r^{Nt} - \underset{d,ly}{\overset{t\to \ell}{M}} \right) = 0 \tag{23}$$

222 $$\frac{\partial \left[\left(1 - \varepsilon^t \right) \omega^{ox} \right]}{\partial t} + \frac{1}{r^2}\frac{\partial}{\partial r}\left(r^2 \varepsilon^t \omega^{ox} \frac{k}{\mu^\ell} \Sigma' \frac{\partial \varepsilon^t}{\partial r} \right) - \frac{1}{r^2}\frac{\partial}{\partial r}\left[r^2 \left(1 - \varepsilon^t \right) D^{ox} \frac{\partial \omega^{ox}}{\partial r} \right] + \frac{1}{\rho} \underset{ox}{\overset{ox\to t}{M}} = 0 \tag{24}$$

223 $$\frac{\partial\left[\left(1-\varepsilon^t\right)\omega^{ch}\right]}{\partial t}+\frac{1}{r^2}\frac{\partial}{\partial r}\left(r^2\varepsilon^t\omega^{ch}\frac{k}{\mu^{\ell}}\Sigma'\frac{\partial\varepsilon^t}{\partial r}\right)-\frac{1}{r^2}\frac{\partial}{\partial r}\left[r^2\left(1-\varepsilon^t\right)D^{ch}\frac{\partial\omega^{ch}}{\partial r}\right]+\frac{1}{\rho}\overset{ch\to t}{M}_{ch}=0 \qquad (25)$$

224 We have adopted spherical symmetry, and r is the radial coordinate over the spheroid radius. The
225 parameters k and μ^l are the intrinsic permeability of the cellular scaffold and the dynamic viscosity
226 of IF, respectively. They arise by assuming Darcy's law for the relative velocity of the two phases
227 (Mascheroni et al., 2016; Sciumè et al., 2013). Moreover, we take the phases to be incompressible
228 and assign a common value for their densities, which we denote by the constant ρ. Note that this
229 leads to $\alpha_B=1$. Then, we model the growth of the spheroid as a free-boundary problem, where the
230 interface constituted by TCs is a material surface for the TCs that moves with velocity v^t, given by:

231 $$\frac{dR}{dt}=v^t=-\frac{k}{\mu^{\ell}}\Sigma'\left.\frac{\partial\varepsilon^t}{\partial r}\right|_{r=R} \qquad (26)$$

232 where R is the external radius of the spheroid. The closed form of the differential problem is then
233 obtained by defining a proper set of boundary and initial conditions. In particular, regularity at the
234 spheroid center requires:

235 $$\frac{\partial\varepsilon^t}{\partial r}=\frac{\partial\omega^{Nt}}{\partial r}=\frac{\partial\omega^{ox}}{\partial r}=\frac{\partial\omega^{ch}}{\partial r}=0,\quad \text{in } r=0, \qquad (27)$$

236 while we enforce Dirichlet boundary conditions on the tumor external surface:

237 $$\varepsilon^t=\varepsilon^t_{ext},\quad \omega^{Nt}=0,\quad \omega^{ox}=\omega^{ox}_{env},\quad \omega^{ch}=\omega^{ch}_{env},\quad \text{in } r=R. \qquad (28)$$

238 Finally, we assume the following initial conditions over the spheroid radius:

239 $$\varepsilon^t=\varepsilon^t_{ext},\quad \omega^{Nt}=0,\quad \omega^{ox}=\omega^{ox}_{env},\quad \omega^{ch}=0,\quad \text{on } 0<r<R \text{ at } t=0. \qquad (29)$$

240

241 *2.4 Model parameters*

242 The parameters used in the model are listed in Table 1. Some of the values are taken from
243 (Mascheroni et al., 2016), where the model results are compared to experimental data. In this work,
244 we need to add the values for the parameters appearing in the equations governing drug transport
245 and uptake. For these quantities we assume the values in (Frieboes et al., 2009), obtained for
246 spheroids treated with Doxorubicin. Actually, the parameter governing drug-induced cell death,

λ_{ch}^{t}, depends on the particular therapeutic agent and cell line that are considered. Here it is selected to produce a reasonable response of the model when the spheroids are subjected to the given drug concentrations. Note that, as it will be shown in Section 3.3, model results will not be significantly affected by this choice.

Table 1 Parameters used in the model.

Parameter	Value	Unit	Reference
ω_{env}^{ox}	7.7×10^{-6}	(-)	(Mueller-Klieser et al., 1986; Mueller-Klieser and Sutherland, 1982)
c^{ox}	1.48×10^{-7}	(-)	(Casciari et al., 1992a, 1992b)
γ_0^t	3.0×10^{-4}	$\mathrm{kg/(m^3\cdot s)}$	(Casciari et al., 1992a, 1992b)
β	0.5	(-)	(Byrne and Preziosi, 2003)
ε_n^t	0.8	(-)	(Byrne and Preziosi, 2003)
ε_0^t	$1/3$	(-)	(Byrne and Preziosi, 2003)
k	1.8×10^{-15}	$\mathrm{m^2}$	(Netti et al., 2000)
μ^{ℓ}	1.0×10^{-3}	$\mathrm{Pa\cdot s}$	(Sciumè et al., 2013b)
D^{ox}	3.2×10^{-9}	$\mathrm{m^2/s}$	(Sciumè et al., 2013b)
ρ	1.0×10^{3}	$\mathrm{kg/m^3}$	(Sciumè et al., 2013b)
ω_{crit}^{ox}	2.0×10^{-6}	(-)	(Mascheroni et al., 2016)
γ_g^t	5.4×10^{-3}	$\mathrm{kg/(m^3\cdot s)}$	(Mascheroni et al., 2016)
γ_n^t	1.5×10^{-1}	$\mathrm{kg/(m^3\cdot s)}$	(Mascheroni et al., 2016)
λ_{ℓ}^t	1.15×10^{-2}	$\mathrm{kg/(m^3\cdot s)}$	(Mascheroni et al., 2016)
α	1.0×10^{5}	Pa	(Mascheroni et al., 2016)
ω_{env}^{ch}	$8.696\div271.76\times10^{-9}$	(-)	(Frieboes et al., 2009)
D^{ch}	9.375×10^{-14}	$\mathrm{m^2/s}$	(Frieboes et al., 2009)
γ_{ch}^t	1.157×10^{-2}	$\mathrm{kg/(m^3\cdot s)}$	(Frieboes et al., 2009)
λ_{ch}^t	5.0×10^{4}	$\mathrm{kg/(m^3\cdot s)}$	(-)

3. Results

3.1 Tumor spheroid growth in the presence of a drug

In this section we test the effects of a drug that targets cell proliferation in a three-dimensional cell aggregate. We consider first tumor spheroids that grow suspended in culture medium, subject to different drug concentrations. We assume drug concentration at spheroid boundary to start from zero and, following a ramp, to reach the final value ω_{env}^{ch} after 3h.

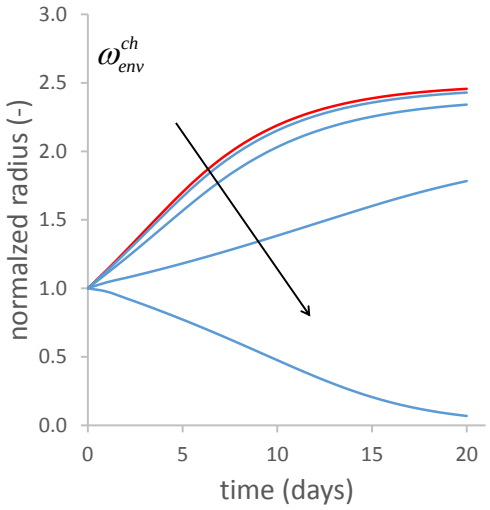

Figure 2 Effect of different drug concentrations on spheroid growth. The red line refers to a spheroid grown in the absence of drug. The other lines are for $\omega_{env}^{ch} = 0.086, 0.347, 1.391, 2.717 \times 10^{-7}$.

In Figure 2, we show the evolution of the spheroid radius over time for different drug mass fractions (i.e. $\omega_{env}^{ch} = 0.086, 0.347, 1.391, 2.717 \times 10^{-7}$). Here, the arrow points in the direction of increasing ω_{env}^{ch}. We consider the normalized value of the spheroid radius, namely the ratio between the present value of the radius and the initial radius of the spheroid (200 μm in this case). The red line represents a spheroid grown in the absence of drug. We can distinguish between the first stages of growth, displaying an exponential/linear behavior, followed by a phase of growth saturation where the radius tends to a steady value. Low concentrations of drug do not alter the shape of the growth curve, whereas for high levels of the chemotherapeutic agent the spheroid starts to shrink and, for the highest value of ω_{env}^{ch}, growth is almost completely inhibited. This behavior closely resembles the growth curves obtained for example in (Kim et al., 2010; Mikhail et al., 2013), where spheroids from various cell lines are subject to different drugs.

Figure 3 shows the drug mass fraction inside the spheroid for an intermediate value of ω_{env}^{ch}, at the end of the simulation. Note the steep gradient of drug appearing from the boundary towards the center of the cell aggregate. In this case, the therapeutic agent can exert its effect only over the outermost region of the spheroid. This phenomenon arises as a consequence of poor diffusion of the drug molecules inside the spheroid and due to drug uptake by proliferating TCs. Interestingly, similar results are obtained in the experimental literature (see for example (Gong et al., 2015; Wang et al., 2013)), analyzing the penetration of free drug into a spheroid.

Then, we look for the value of drug mass fraction that is able to provide a reduction of 50% in spheroid volume (usually identified with the label IC_{50}, for "half maximal inhibitory concentration" (Curtis et al., 2016)). We find a value of $\omega_{env}^{ch} = 1.185 \times 10^{-7}$, which we will denote from now on with IC_{50}. The growth curve relative to this drug mass fraction is shown in Figure 4.a, where we report the evolution of the normalized volume (i.e. the ratio between the spheroid volume and its initial volume) over time. The evolution of oxygen mass fraction over the spheroid radius is represented in Figure 4.b. Note the steep oxygen gradients at later times of the simulation, from the spheroid boundary towards its interior. The necrotic mass fraction of TCs is displayed in Figure 4.c. A necrotic population appears after a few days from the beginning of the simulation and gives rise to a necrotic core at later days. Both Figures 4.b and 4.c refer to a spheroid not treated with the drug, whereas the second row of Figures (4.d-f) pertains to a spheroid grown in the presence of a drug with a mass fraction equal to IC_{50}. The drug mass fraction over the spheroid radius is presented in Figure 4.d. Note that, after a few days from the beginning of the simulation, the therapeutic agent is mainly distributed over the spheroid periphery. Figure 4.e shows the oxygen mass fraction in the drug-treated spheroid. We can observe a behavior similar to the one in Figure 4.b, but this time over a smaller spheroid. Finally, the necrotic mass fraction in a spheroid subjected to the drug is shown in Figure 4.f. Compared to Figure 4.c, here the necrotic core is less extended and appears at later times in the simulation. This may be due to a smaller mass fraction of LTCs that can undergo necrosis, deriving from LTC killing by the chemotherapeutic agent.

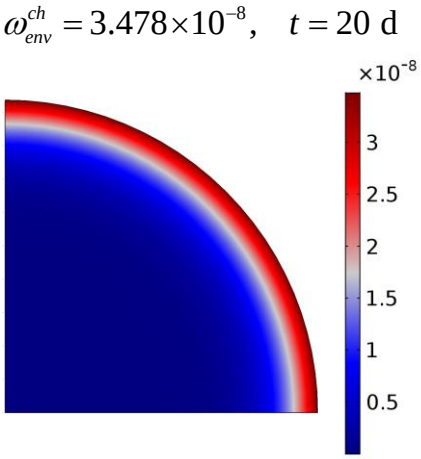

Figure 3 Drug mass fraction inside the spheroid at day 20 and for $\omega_{env}^{ch} = 3.478\times10^{-8}$.

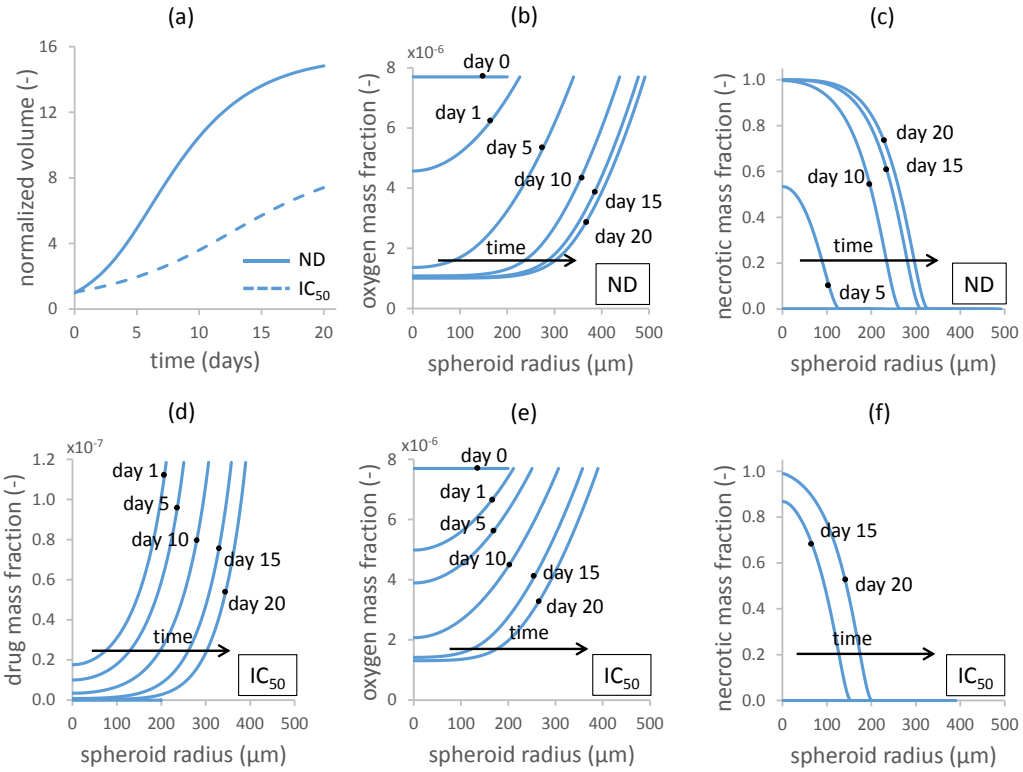

Figure 4 Comparison between a spheroid grown without an external drug (ND) and one treated with a drug mass fraction equal to IC_{50}.

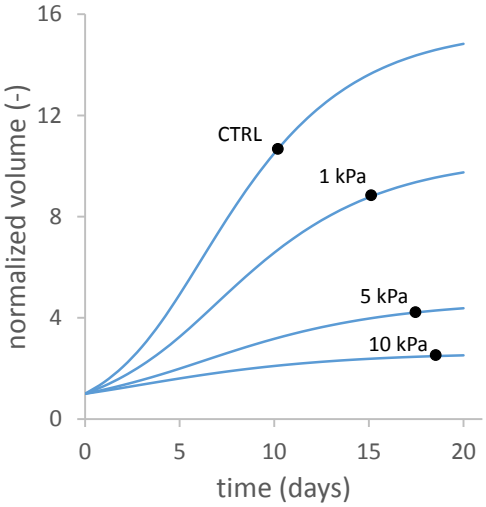

Figure 5 Normalized volumes of spheroids grown under different external mechanical pressures.

3.2 Effect of mechanical compression on drug efficacy

In (Mascheroni et al., 2016), we investigated the effects of an external mechanical pressure on the growth curves of tumor spheroids. Figure 5 report these previous findings, in terms of the evolution of the normalized volumes of spheroids subjected to different compressive stresses. We consider four compression levels, ranging from 1kPa to 10kPa. The growth of the most compressed spheroid shows a 7-fold reduction when compared to the control case (grown in the absence of an external stress). Note that the inhibitory effect of compressive stresses is included in the equations through the constitutive relation in (14). We make use of these results to test our newly introduced framework for drug transport and uptake in the spheroid. In particular, we apply the same external mass fraction of drug (IC_{50}) to each of the compression tests. Then, we check for variations in spheroid volumes with respect to the case with no drug added to the culture medium (Figure 6 and 7). Figure 6 compares the normalized volumes of spheroids undergoing different compressive stresses. We test spheroids in the absence (ND) or presence (IC_{50}) of a chemotherapeutic drug. Both the series, ND and IC_{50}, exhibit the same decreasing trend, although with a slower volume reduction for drug-treated spheroids. The variation between the two volumes for each compressive condition is shown in Figure 7. According to the definition of IC_{50}, the control case displays a 50% reduction in volume. Interestingly, the series exhibit a percentage variation decreasing with the extent of mechanical compression, as highlighted by the black arrow. The case undergoing maximum compression shows a reduction of about 30% in volume reduction. The observed behavior arises as a consequence of a lower proliferation index within the spheroid. In fact, mechanical stress inhibits

cell proliferation via equation (14) of the model, providing smaller values for the growth term as compression increases. Since our discussion is based on drugs that target cell duplication, growth inhibition is responsible for a cell population over which the therapeutic agent is less effective. Note that this effect could be relevant for *in vivo* applications: a drug concentration that is known to be effective in a particular regime (such as 3D cultures) could not provide the same results when the tumor is subjected to mechanical compression. Moreover, since several drug screenings are evaluated on monolayer cultures, such effects arising from a full three-dimensional setting may be overlooked (Friedrich et al., 2009).

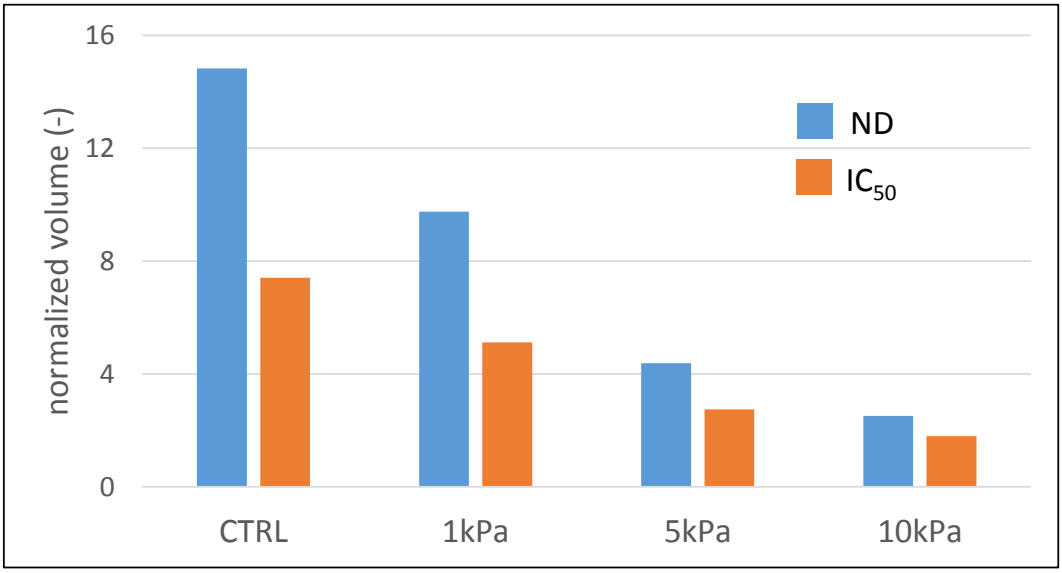

Figure 6 Comparison of the normalized volumes of spheroids subject to different mechanical stress, grown in the absence of drug (ND) or subject to a drug concentration of IC_{50}.

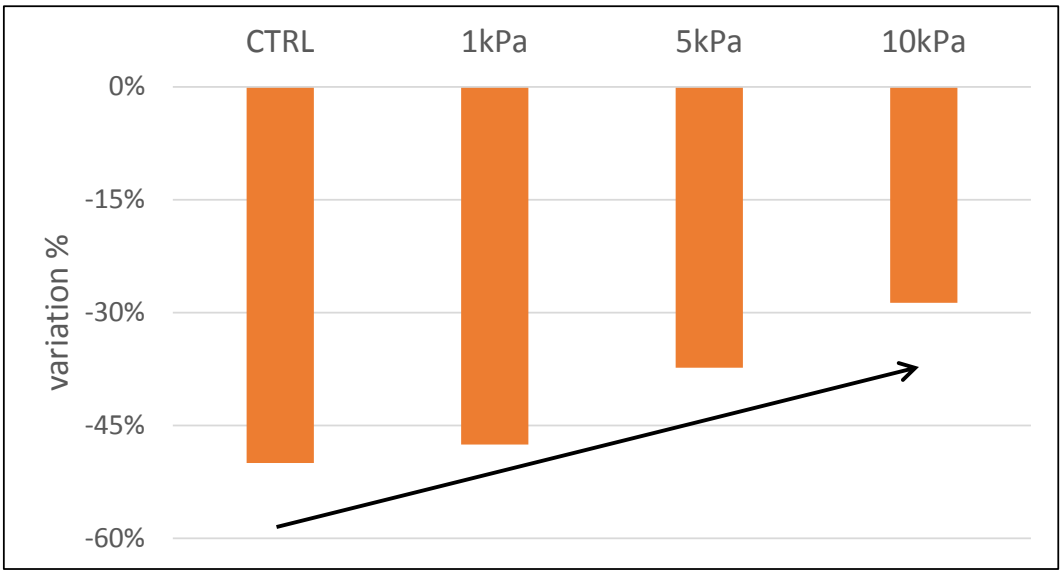

Figure 7 Variation in spheroid volume due to the action of a chemotherapeutic drug at different external mechanical pressures. As shown by the arrow, the efficacy of proliferation targeting drugs is less effective for higher tumor compressions, because of stress inhibition of growth.

3.3 Response of the model for different forms of the drug-induced death term

To confirm that model results are not biased by the particular choice of the term in (17), we test different mathematical expressions accounting for drug-induced cell death. The simplest hypothesis, assumed in (17), considers cell death to be proportional to the local amount of drug. In the following, we will refer to this case as the "linear" one. We introduce two additional relationships, given by:

$$\underset{d,ch}{\overset{t\to\ell}{M}} = f_{ch}\frac{m_1\omega^{ch}}{\omega^{ch}+m_2}\omega^{Lt}\varepsilon^{t} \tag{30}$$

$$\underset{d,ch}{\overset{t\to\ell}{M}} = f_{ch}\,p_1\left(\omega^{ch}\right)^{p_2}\omega^{Lt}\varepsilon^{t} \tag{31}$$

In (30), we assume a dependence of the Michaelis-Menten type; in (31) the assumed relationship takes the form of a power law. Note that, as the functional dependence on the local drug concentration changes, these relations give rise to new values for the inhibitory concentration IC_{50}. We report the new IC_{50} and the values for the parameters that characterize the above expressions in Table 2. Once the new forms for the drug-induced cell death term are implemented into the model, we perform the same numerical tests of the previous section to analyze the coupled effect of drug action and mechanical compression. In Figure 8, we report the variation in terms of spheroid volume induced by the drug for different compressive stresses. Like in the previous Figure, the first series of data serves as a control and indicates a variation of 50% with respect to the drug-free condition. The other series are related to the different compression regimes and compare the model response for the different mathematical relationships assumed for the death term. It is possible to observe that the variation in volume reduction is similar to the linear case, analyzed in the previous section. The effect of mechanical compression on drug efficacy described previously does not seem therefore to be originated from the particular mathematical form adopted for the death term.

Table 2 Parameter values for the relations assumed in the cell death term.

Relation	Parameter	Value	Unit	IC_{50}
Linear	λ_{ch}^{t}	5.0×10^{4}	$\mathrm{kg}/(\mathrm{m}^3\cdot\mathrm{s})$	1.185×10^{-7}
Michaelis-Menten	m_1	1.5×10^{-2}	$\mathrm{kg}/(\mathrm{m}^3\cdot\mathrm{s})$	5.345×10^{-8}
	m_2	1.0×10^{-7}	$(-)$	
Power law	p_1	2.5×10^{11}	$\mathrm{kg}/(\mathrm{m}^3\cdot\mathrm{s})$	1.862×10^{-7}
	p_2	2	$(-)$	

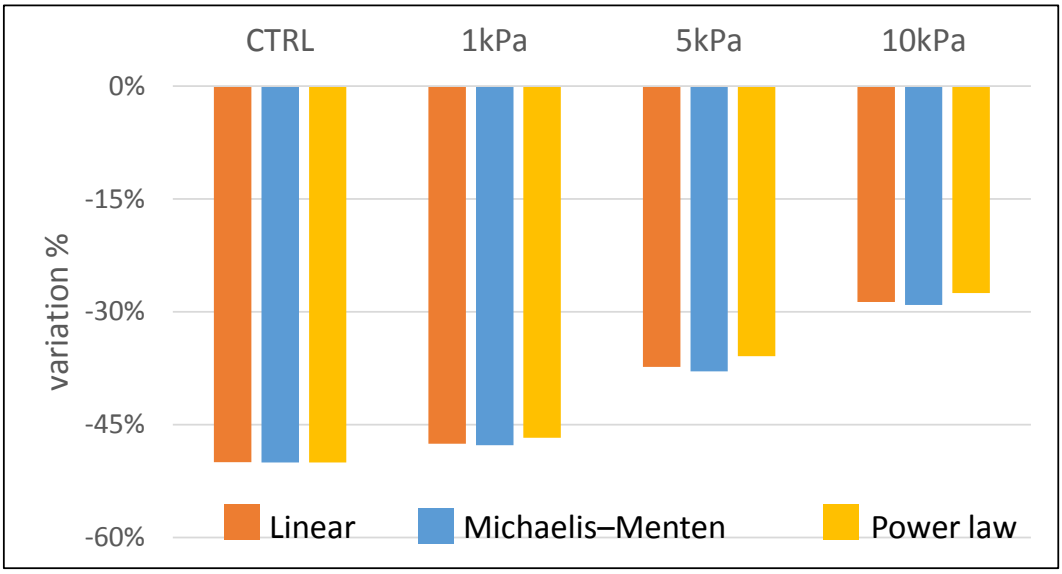

Figure 8 Effect of different mathematical relations on spheroid volume variation.

4. Conclusion

In this work, we introduce equations for drug transport and uptake by TCs in our previous mathematical model for avascular tumor growth. Then, we adapt the equations for the tumor spheroid case and test the effects of a proliferation targeting drug on spheroid growth curves. We observe a qualitative agreement between model results and experimental literature (Gong et al., 2015; Kim et al., 2010; Mikhail et al., 2013; Wang et al., 2013). Then, we simulate tumor spheroids undergoing mechanical compressive stresses of different amplitudes and consider their volume reduction due to the presence of a therapeutic agent. Interestingly, we notice a decreased growth inhibition efficacy of the drug in terms of the final volumes reached by the spheroids, arising because of compressive stresses. Finally, we test three different mathematical expressions for the cell death term induced by the therapeutic agent. The resulting predictions are similar for all the tested relations, suggesting that the particular form of the adopted constitutive relation does not influence model response. Taken together, these results suggest that mechanical compression of tumor spheroids may compromise the efficacy of a chemotherapeutic agent targeting cell proliferation.

As several simplifying assumptions are considered in the work, the model is certainly open to further improvements. In particular, here we model only one nutrient species, i.e. oxygen, diffusing in the interstitial fluid and regulating TC proliferation. Even though the presence of other chemicals is implicitly contained within the mass exchange term in (14), future inclusion of additional nutrients, growth and necrosis factors could provide a more detailed description of the tumor system (Chauhan and Jain, 2013; Jain et al., 2014). Moreover, since the particular physicochemical environment in which the tumor is embedded affects significantly the outcomes of therapies (see for example (Luk et al., 1990), (Seebacher et al., 2015)), proper consideration of these factors would result in a better description of drug dynamics. Notably, some experiments couple therapeutic agents to nanoparticle formulations, enabling a larger penetration into the tumor (Kim et al., 2010; Wang et al., 2013). Note that this latter kind of results can be integrated in the current model, once suitable mechanisms for nanoparticle delivery are hypothesized. Another point requiring some attention is the proper choice of constitutive relations. As it happens frequently in literature, most of these laws are derived from phenomenological arguments. More experimental work is needed to link the mathematical form assigned to the various terms to the underlying biology. This kind of reasoning should be applied to the constitutive relations accounting for the drug uptake and the following effects on TCs, as well as the mechanical description of the tumor ensemble. For the latter,

here we consider a simple law, linking the stress in the tissue to the local volume fraction of tumor cells. This assumption provides a great simplification of the equations and is shown to give a good description of experimental observations (Mascheroni et al., 2016). However, it neglects several phenomena related to the mechanical behavior of a biological tissue. For example, viscoplastic effects existing at smaller timescales than those of cell proliferation are not taken into account (Forgacs et al., 1998; Giverso and Preziosi, 2012). Also, breaking and formation of cellular bonds during tumor development should be included to give a more complete description (Ambrosi et al., 2012; Preziosi et al., 2010). Finally, we highlight the need for experiments addressing the interactions between therapeutic agents and tumor mechanical environment. These experiments will serve to calibrate the parameters in the equations and to test model results. Part of future experimental work should also be devoted to the biochemical understanding of the growth inhibition process following mechanical stress. Although some work is already present in the literature (Cheng et al., 2009; Delarue et al., 2014; Loessner et al., 2013), several details remain to be elucidated. New investigations analyzing the interactions between the tumor and its bio-mechanical environment should allow for a better understanding of disease progression, with the final goal of aiding the design of effective therapeutic treatments.

Acknowledgements

-

References

Abercrombie, M., Ambrose, E.J., 1962. The surface properties of cancer cells: a review. Cancer Res. 22, 525–48.

Altrock, P.M., Liu, L.L., Michor, F., 2015. The mathematics of cancer: integrating quantitative models. Nat. Rev. Cancer 15, 730–745. doi:10.1038/nrc4029

Ambrosi, D., Preziosi, L., Vitale, G., 2012. The interplay between stress and growth in solid tumors. Mech. Res. Commun. 42, 87–91. doi:10.1016/j.mechrescom.2012.01.002

Butcher, D.T., Alliston, T., Weaver, V.M., 2009. A tense situation: forcing tumour progression. Nat. Rev. Cancer 9, 108–122. doi:10.1038/nrc2544

Byrne, H., Preziosi, L., 2003. Modelling solid tumour growth using the theory of mixtures. Math. Med. Biol. 20, 341–66. doi:10.1093/imammb/20.4.341

Byrne, H.M., 2010. Dissecting cancer through mathematics: from the cell to the animal model. Nat. Rev. Cancer 10, 221–30. doi:10.1038/nrc2808

Casciari, J.J., Sotirchos, S. V, Sutherland, R.M., 1992a. Mathematical modelling of microenvironment and growth in EMT6/Ro multicellular tumour spheroids. Cell Prolif. 25, 1–22. doi:10.1111/j.1365-2184.1992.tb01433.x

Casciari, J.J., Sotirchos, S. V, Sutherland, R.M., 1992b. Variations in tumor cell growth rates and metabolism with oxygen concentration, glucose concentration, and extracellular pH. J. Cell. Physiol. 151, 386–94. doi:10.1002/jcp.1041510220

Chauhan, V.P., Jain, R.K., 2013. Strategies for advancing cancer nanomedicine. Nat. Mater. 12, 958–62. doi:10.1038/nmat3792

462 Cheng, G., Tse, J., Jain, R.K., Munn, L.L., 2009. Micro-environmental mechanical stress controls tumor spheroid size and morphology
463 by suppressing proliferation and inducing apoptosis in cancer cells. PLoS One 4, e4632. doi:10.1371/journal.pone.0004632

464 Curtis, L.T., England, C.G., Wu, M., Lowengrub, J., Frieboes, H.B., 2016. An interdisciplinary computational/experimental approach
465 to evaluate drug-loaded gold nanoparticle tumor cytotoxicity. Nanomedicine 11, 197–216. doi:10.2217/nnm.15.195

466 Dawidczyk, C.M., Kim, C., Park, J.H., Russell, L.M., Lee, K.H., Pomper, M.G., Searson, P.C., 2014. State-of-the-art in design rules for
467 drug delivery platforms: lessons learned from FDA-approved nanomedicines. J. Control. Release 187, 133–44.
468 doi:10.1016/j.jconrel.2014.05.036

469 Delarue, M., Montel, F., Vignjevic, D., Prost, J., Joanny, J.-F., Cappello, G., 2014. Compressive stress inhibits proliferation in tumor
470 spheroids through a volume limitation. Biophys. J. 107, 1821–8. doi:10.1016/j.bpj.2014.08.031

471 Dietrich, C., Wallenfang, K., Oesch, F., Wieser, R., 1997. Differences in the mechanisms of growth control in contact-inhibited and
472 serum-deprived human fibroblasts. Oncogene 15, 2743–7. doi:10.1038/sj.onc.1201439

473 Fernández-Sánchez, M.E., Barbier, S., Whitehead, J., Béalle, G., Michel, A., Latorre-Ossa, H., Rey, C., Fouassier, L., Claperon, A.,
474 Brullé, L., Girard, E., Servant, N., Rio-Frio, T., Marie, H., Lesieur, S., Housset, C., Gennisson, J.-L., Tanter, M., Ménager, C., Fre,
475 S., Robine, S., Farge, E., 2015. Mechanical induction of the tumorigenic β-catenin pathway by tumour growth pressure.
476 Nature 523, 92–95. doi:10.1038/nature14329

477 Forgacs, G., Foty, R. a, Shafrir, Y., Steinberg, M.S., 1998. Viscoelastic properties of living embryonic tissues: a quantitative study.
478 Biophys. J. 74, 2227–34. doi:10.1016/S0006-3495(98)77932-9

479 Frieboes, H.B., Edgerton, M.E., Fruehauf, J.P., Rose, F.R.A.J., Worrall, L.K., Gatenby, R. a, Ferrari, M., Cristini, V., 2009. Prediction of
480 drug response in breast cancer using integrative experimental/computational modeling. Cancer Res. 69, 4484–92.
481 doi:10.1158/0008-5472.CAN-08-3740

482 Friedrich, J., Seidel, C., Ebner, R., Kunz-Schughart, L.A., 2009. Spheroid-based drug screen: considerations and practical approach.
483 Nat. Protoc. 4, 309–324. doi:10.1038/nprot.2008.226

484 Giverso, C., Preziosi, L., 2012. Modelling the compression and reorganization of cell aggregates. Math. Med. Biol. 29, 181–204.
485 doi:10.1093/imammb/dqr008

486 Gong, X., Lin, C., Cheng, J., Su, J., Zhao, H., Liu, T., Wen, X., Zhao, P., 2015. Generation of Multicellular Tumor Spheroids with
487 Microwell-Based Agarose Scaffolds for Drug Testing. PLoS One 10, e0130348. doi:10.1371/journal.pone.0130348

488 Goodman, T.T., Chen, J., Matveev, K., Pun, S.H., 2008. Spatio-temporal modeling of nanoparticle delivery to multicellular tumor
489 spheroids. Biotechnol. Bioeng. 101, 388–399. doi:10.1002/bit.21910

490 Helmlinger, G., Netti, P.A., Lichtenbeld, H.C., Melder, R.J., Jain, R.K., 1997. Solid stress inhibits the growth of multicellular tumor
491 spheroids. Nat. Biotechnol. 15, 778–83. doi:10.1038/nbt0897-778

492 Hengst, L., Dulic, V., Slingerland, J.M., Lees, E., Reed, S.I., 1994. A cell cycle-regulated inhibitor of cyclin-dependent kinases. Proc.
493 Natl. Acad. Sci. U. S. A. 91, 5291–5. doi:10.1073/pnas.91.12.5291

494 Hossain, S.S., Hossainy, S.F. a., Bazilevs, Y., Calo, V.M., Hughes, T.J.R., 2012. Mathematical modeling of coupled drug and drug-
495 encapsulated nanoparticle transport in patient-specific coronary artery walls. Comput. Mech. 49, 213–242.
496 doi:10.1007/s00466-011-0633-2

497 Jain, R.K., Martin, J.D., Stylianopoulos, T., 2014. The role of mechanical forces in tumor growth and therapy. Annu. Rev. Biomed.
498 Eng. 16, 321–46. doi:10.1146/annurev-bioeng-071813-105259

499 Kim, M., Gillies, R.J., Rejniak, K. a, 2013. Current Advances in Mathematical Modeling of Anti-Cancer Drug Penetration into Tumor
500 Tissues. Front. Oncol. 3, 278. doi:10.3389/fonc.2013.00278

501 Kim, T.-H., Mount, C.W., Gombotz, W.R., Pun, S.H., 2010. The delivery of doxorubicin to 3-D multicellular spheroids and tumors in a
502 murine xenograft model using tumor-penetrating triblock polymeric micelles. Biomaterials 31, 7386–97.
503 doi:10.1016/j.biomaterials.2010.06.004

504 Kim, Y., Stolarska, M. a., Othmer, H.G., 2011. The role of the microenvironment in tumor growth and invasion. Prog. Biophys. Mol.
505 Biol. 106, 353–79. doi:10.1016/j.pbiomolbio.2011.06.006

506 Lewis, R.W., Schrefler, B.A., 1998. The finite element method in the static and dynamic deformation and consolidation of porous
507 media. John Wiley.

508 Loessner, D., Flegg, J. a, Byrne, H.M., Clements, J. a, Hutmacher, D.W., 2013. Growth of confined cancer spheroids: a combined
509 experimental and mathematical modelling approach. Integr. Biol. 5, 597. doi:10.1039/c3ib20252f

510 Luk, C.K., Veinot-Drebot, L., Tjan, E., Tannock, I.F., 1990. Effect of transient hypoxia on sensitivity to doxorubicin in human and
511 murine cell lines. J. Natl. Cancer Inst. 82, 684–92. doi:10.1093/jnci/82.8.684

512 Mascheroni, P., Stigliano, C., Carfagna, M., Boso, D.P., Preziosi, L., Decuzzi, P., Schrefler, B.A., 2016. Predicting the growth of
513 glioblastoma multiforme spheroids using a multiphase porous media model. Biomech. Model. Mechanobiol. 15, 1215–28.
514 doi:10.1007/s10237-015-0755-0

515 Mikhail, A.S., Eetezadi, S., Allen, C., 2013. Multicellular tumor spheroids for evaluation of cytotoxicity and tumor growth inhibitory

effects of nanomedicines in vitro: a comparison of docetaxel-loaded block copolymer micelles and Taxotere®. PLoS One 8, e62630. doi:10.1371/journal.pone.0062630

Montel, F., Delarue, M., Elgeti, J., Vignjevic, D., Cappello, G., Prost, J., 2012. Isotropic stress reduces cell proliferation in tumor spheroids. New J. Phys. 14, 55008. doi:10.1088/1367-2630/14/5/055008

Mpekris, F., Angeli, S., Pirentis, A.P., Stylianopoulos, T., 2015. Stress-mediated progression of solid tumors: effect of mechanical stress on tissue oxygenation, cancer cell proliferation, and drug delivery. Biomech. Model. Mechanobiol. 14, 1391–402. doi:10.1007/s10237-015-0682-0

Mueller-Klieser, W., 2000. Tumor biology and experimental therapeutics. Crit. Rev. Oncol. Hematol. 36, 123–39.

Mueller-Klieser, W., Freyer, J.P., Sutherland, R.M., 1986. Influence of glucose and oxygen supply conditions on the oxygenation of multicellular spheroids. Br. J. Cancer 53, 345–53.

Mueller-Klieser, W.F., Sutherland, R.M., 1982. Oxygen tensions in multicell spheroids of two cell lines. Br. J. Cancer 45, 256–64.

Netti, P.A., Berk, D.A., Swartz, M.A., Grodzinsky, A.J., Jain, R.K., 2000. Role of extracellular matrix assembly in interstitial transport in solid tumors. Cancer Res. 60, 2497–503.

Pinder, G.F., Gray, W.G., 2008. Essentials of Multiphase Flow and Transport in Porous Media, 1st ed. John Wiley & Sons, Hoboken, New Jersey. doi:10.1002/9780470380802

Planas-Silva, M.D., Weinberg, R.A., 1997. The restriction point and control of cell proliferation. Curr. Opin. Cell Biol. 9, 768–72. doi:10.1016/S0955-0674(97)80076-2

Polyak, K., Kato, J.Y., Solomon, M.J., Sherr, C.J., Massague, J., Roberts, J.M., Koff, A., 1994. p27Kip1, a cyclin-Cdk inhibitor, links transforming growth factor-beta and contact inhibition to cell cycle arrest. Genes Dev. 8, 9–22. doi:10.1101/gad.8.1.9

Preziosi, L., Ambrosi, D., Verdier, C., 2010. An elasto-visco-plastic model of cell aggregates. J. Theor. Biol. 262, 35–47. doi:10.1016/j.jtbi.2009.08.023

Preziosi, L., Tosin, A., 2009. Multiphase and multiscale trends in cancer modelling. Math. Model. Nat. Phenom. 4, 1–11. doi:10.1051/mmnp/20094301

Sciumè, G., Gray, W.G., Ferrari, M., Decuzzi, P., Schrefler, B.A., 2013. On Computational Modeling in Tumor Growth. Arch. Comput. Methods Eng. 20, 327–352. doi:10.1007/s11831-013-9090-8

Sciumè, G., Shelton, S., Gray, W., Miller, C., Hussain, F., Ferrari, M., Decuzzi, P., Schrefler, B., 2013. A multiphase model for three-dimensional tumor growth. New J. Phys. 15, 15005. doi:10.1088/1367-2630/15/1/015005

Seebacher, N.A., Richardson, D.R., Jansson, P.J., 2015. Glucose modulation induces reactive oxygen species and increases P-glycoprotein-mediated multidrug resistance to chemotherapeutics. Br. J. Pharmacol. 172, 2557–2572. doi:10.1111/bph.13079

St Croix, B., Florenes, V.A., Rak, J.W., Flanagan, M., Bhattacharya, N., Slingerland, J.M., Kerbel, R.S., 1996. Impact of the cyclin-dependent kinase inhibitor p27Kip1 on resistance of tumor cells to anticancer agents. Nat. Med. 2, 1204–10.

St Croix, B., Sheehan, C., Rak, J.W., Florenes, V. a, Slingerland, J.M., Kerbel, R.S., 1998. E-Cadherin-dependent growth suppression is mediated by the cyclin-dependent kinase inhibitor p27(KIP1). J. Cell Biol. 142, 557–71. doi:10.1083/jcb.142.2.557

Stylianopoulos, T., Martin, J.D., Chauhan, V.P., Jain, S.R., Diop-Frimpong, B., Bardeesy, N., Smith, B.L., Ferrone, C.R., Hornicek, F.J., Boucher, Y., Munn, L.L., Jain, R.K., 2012. Causes, consequences, and remedies for growth-induced solid stress in murine and human tumors. Proc. Natl. Acad. Sci. 109, 15101–15108. doi:10.1073/pnas.1213353109

Trédan, O., Galmarini, C.M., Patel, K., Tannock, I.F., 2007. Drug resistance and the solid tumor microenvironment. J. Natl. Cancer Inst. 99, 1441–54. doi:10.1093/jnci/djm135

Vinci, M., Gowan, S., Boxall, F., Patterson, L., Zimmermann, M., Court, W., Lomas, C., Mendiola, M., Hardisson, D., Eccles, S. a, 2012. Advances in establishment and analysis of three-dimensional tumor spheroid-based functional assays for target validation and drug evaluation. BMC Biol. 10, 29. doi:10.1186/1741-7007-10-29

Wang, X., Zhen, X., Wang, J., Zhang, J., Wu, W., Jiang, X., 2013. Doxorubicin delivery to 3D multicellular spheroids and tumors based on boronic acid-rich chitosan nanoparticles. Biomaterials 34, 4667–79. doi:10.1016/j.biomaterials.2013.03.008

Ward, J.P., King, J.R., 2003. Mathematical modelling of drug transport in tumour multicell spheroids and monolayer cultures. Math. Biosci. 181, 177–207.

Weinberg, B.D., Patel, R.B., Exner, A. a., Saidel, G.M., Gao, J., 2007. Modeling doxorubicin transport to improve intratumoral drug delivery to RF ablated tumors. J. Control. Release 124, 11–9. doi:10.1016/j.jconrel.2007.08.023

Xing, H., Wang, S., Hu, K., Tao, W., Li, J., Gao, Q., Yang, X., Weng, D., Lu, Y., Ma, D., 2005. Effect of the cyclin-dependent kinases inhibitor p27 on resistance of ovarian cancer multicellular spheroids to anticancer chemotherapy. J. Cancer Res. Clin. Oncol. 131, 511–519. doi:10.1007/s00432-005-0677-9

Zahreddine, H., Borden, K.L.B., 2013. Mechanisms and insights into drug resistance in cancer. Front. Pharmacol. 4, 28. doi:10.3389/fphar.2013.00028

569